Photo-induced depopulation of the $^{180}Ta^{m}$ isomer via low-lying intermediate states: Structure and astrophysical implications

D. Belic,[1,*] C. Arlandini,[2] J. Besserer,[3] J. de Boer,[3] J. J. Carroll,[4] J. Enders,[5,†] T. Hartmann,[5] F. Käppeler,[2] H. Kaiser,[5,‡] U. Kneissl,[1] E. Kolbe,[6] K. Langanke,[7] M. Loewe,[3] H. J. Maier,[3] H. Maser,[1] P. Mohr,[5] P. von Neumann-Cosel,[5] A. Nord,[1,*] H. H. Pitz,[1] A. Richter,[5] M. Schumann,[2] F.-K. Thielemann,[6] S. Volz,[5] and A. Zilges[5]

[1]*Institut für Strahlenphysik, Universität Stuttgart, D-70569 Stuttgart, Germany*

[2]*Institut für Kernphysik, Forschungszentrum Karlsruhe, D-76021 Karlsruhe, Germany*

[3]*Sektion Physik, Ludwig-Maximilians Universität München, D-85748 Garching, Germany*

[4]*Department of Physics and Astronomy, Youngstown State University, Youngstown, Ohio 44555*

[5]*Institut für Kernphysik, Technische Universität Darmstadt, D-64289 Darmstadt, Germany*

[6]*Institut für Physik, Universität Basel, CH-4056 Basel, Switzerland*

[7]*Institute of Physics and Astronomy, University of Aarhus, DK-8000 Aarhus C, Denmark*

(Received 6 September 2001; published 14 February 2002)

The photo-induced depopulation of the quasistable isomer ($t_{1/2} \geqslant 1.2\times10^{15}$ yr) in ^{180}Ta with angular momentum and parity $J^{\pi}=9^{-}$ at an excitation energy $E_x=75$ keV was studied at the new bremsstrahlung irradiation facility installed at the Stuttgart 4.3 MV DYNAMITRON accelerator in the energy range of bremsstrahlung end point energies between $E_0=0.8$–3.1 MeV. The onset of the isomer depopulation could be observed starting at an end point energy of $E_0 \approx 1$ MeV, i.e., at an intermediate state of ^{180}Ta at or below that energy. Higher-lying intermediate states were found at 1.22, 1.43, 1.55, 1.85, 2.16, 2.40, 2.64, and 2.80 MeV. The extracted integrated cross sections show a remarkably strong depopulation of the $^{180}Ta^{m}$ isomer by photoexcitation. The results are compared with previous experiments and recent quasiparticle-phonon model calculations. Implications of the results for a possible nucleosynthesis of ^{180}Ta in the *s* process and the neutrino process are discussed.

DOI: 10.1103/PhysRevC.65.035801 PACS number(s): 25.20.Dc, 23.20.Lv, 97.10.Cv, 27.70.+q

I. INTRODUCTION AND MOTIVATION

Amongst about 300 naturally occurring isotopes there are only nine with odd proton and odd neutron numbers. The heaviest of them, ^{180}Ta, owes its existence to a low-lying isomer at an excitation energy of 75 keV while the ground state is unstable ($t_{1/2}=8.1$ h), see Fig. 1. The extremely long half-life ($t_{1/2} \geqslant 1.2\times10^{15}$ yr) results from the large spin difference of the aligned coupling of $\pi 9/2[514]+\nu 9/2[624]$ states to a total spin $J^{\pi}=9^{-}$ compared to the antialigned $\pi 7/2[404]$ and $\nu 9/2[624]$ ground-state (g.s.) configuration leading to $J^{\pi}=1^{+}$. The stretched two-quasiparticle nature makes it an interesting candidate in the search for possible structure effects of excitations built on isomers as was done, for example, in studies using targets of the famous 31 yr, $J^{\pi}=16^{+}$ isomer in ^{178}Hf [1–3] or radioactive ^{174m}Hf beams [4]. The natural abundance of ^{180}Ta presents another interesting puzzle. With tantalum being the rarest element and having a relative abundance of 0.012% only, ^{180}Ta is nature's rarest (quasi)stable isotope. Despite its rarity, its nucleosynthesis has been a mystery for a long time because it is bypassed by the main production processes of heavy nuclei [5]. However, two weak paths within the *s* process have been suggested. One possibility would be β decay of the $J^{\pi}=8^{-}$ isomer in ^{180}Hf [6]. However, present experimental limits exclude significant contributions to the ^{180}Ta abundance by this process [7]. Alternatively, low-lying states in ^{179}Hf may β decay to ^{179}Ta under *s*-process conditions, and subsequent neutron capture also leads to ^{180}Ta [8]. The latter scenario requires a temperature of about 3×10^{8} K. In order to quantify this path, the neutron capture cross section of the radioactive ^{179}Ta ($t_{1/2}=665$ d) needs to be measured [9]. The neutron capture cross section of $^{180}Ta^{m}$ recently was

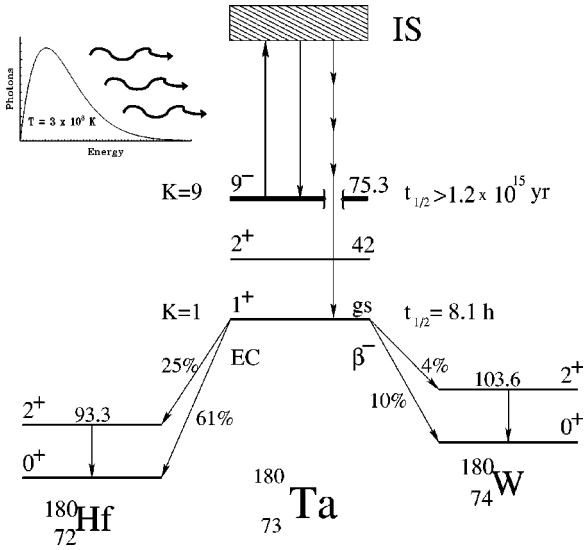

FIG. 1. Low-energy level and decay scheme of ^{180}Ta.

*Present address: Agilent Technologies Deutschland, D-71034 Böblingen, Germany.

†Present address: NSCL, MSU, East Lansing, MI 48824.

‡Present address: Büro Fritz GmbH, D-64683 Einhausen, Germany.

measured in the keV energy range for a detailed *s*-process analysis of the nucleosynthesis of $^{180}Ta^{m}$ [10].

The decay properties of ^{180}Ta may be considerably modified in the stellar environment because of its isomeric nature. The photon bath accompanying the *s* process can depopulate the isomer by resonant photoabsorption into higher-lying intermediate states (IS's) with a branching to the g.s. (typically by a cascade because of the large angular momentum difference). Such an electromagnetic coupling of the isomer and g.s. may destroy all or parts of the synthesized ^{180}Ta. Thus, considerable experimental efforts have been made in recent years to search for IS's of astrophysical relevance.

It may be noted that the resonant depopulation of long-lived isomers is also discussed as a possible driving mechanism for a γ-ray laser [11]. Recently, it has been demonstrated for the nucleus ^{103}Rh that population inversion can be achieved in resonant photoabsorption from bremsstrahlung fields [12]. The nucleus ^{180}Ta is one of the rare cases where typical cross sections can be determined experimentally. This provides a benchmark for the critical discussion (see Refs. [13–15]) of recent work claiming to have observed resonant depopulation of the 31 yr, $J^{\pi}=16^{+}$ isomer in ^{178}Hf by x rays [16]. However, recent experiments by Ahmad *et al.* [17] seem to rule out the results of Ref. [16].

Activation measurements have been performed with real photons from bremsstrahlung [18–20] or strong radioactive sources [20–22] and with Coulomb excitation [23–25]. The principle of detection in the activation experiments is sketched in Fig. 1. After irradiation one searches for population of the g.s. by its specific decay features. The strongest decay branch is by electron capture to the g.s. of ^{180}Hf with the signature of characteristic Hf x rays. There are also weaker branches populating the 2_1^+ states in ^{180}Hf and ^{180}W. Direct information on the energies and cross sections of IS's can only be extracted from measurements of excitation functions with photon beams of variable energy.

Alternatively, ^{180}Ta has been studied recently in great detail by γ spectroscopy [26–32]. Contrary to high-spin studies after fusion-evaporation reactions, these investigations used light-ion and light heavy-ion incomplete fusion reactions to enhance the sensitivity in the spin window around $J=9$ of interest here. A wealth of spectroscopic data has been obtained, but only recently has there been a concrete suggestion [33] of a connection between levels and transitions seen in the spectroscopic data and the intermediate states observed in photoactivation experiments. Additionally, in-beam Coulomb excitation experiments were performed [34,35]. A recent study demonstrates population of the g.s. following Coulomb excitation, but the IS could not be identified so far [35].

All scattering experiments off ^{180}Ta are limited by the extremely low natural abundance of ^{180}Ta. Here, we report a new photo-induced depopulation experiment using the world's resources of enriched (to 5.45%) ^{180}Ta material. Data were taken at the high-current Dynamitron accelerator at Stuttgart with a setup optimized for the off-line activation detection [36]. This allowed for the first time to extract IS's down to $E_x \approx 1$ MeV. The astrophysical consequences for a possible *s*-process production have been discussed elsewhere [38]. Additionally, nuclear resonance fluorescence (NRF) measurements have been performed with the enriched target to search for decay branches of IS's back to the $J^{\pi}=9^{-}$ isomer. The present work provides a full account of the experimental results and discusses their nuclear structure and astrophysical implications.

II. PHOTOACTIVATION AND PHOTON SCATTERING TECHNIQUES USING BREMSSTRAHLUNG

Photoactivation (depopulation or population of long-lived isomers in photo-induced reactions) and photon scattering off bound nuclear states (nuclear resonance fluorescence) share the principal advantage of a well-known reaction mechanism. Model-independent information can be extracted from both kinds of experiments since both the excitation (photoabsorption) and deexcitation processes (electromagnetic decays) proceed via the well-known electromagnetic interaction.

A. Photoactivation of isomers

Isomeric states which differ substantially in spin from the ground state cannot be depopulated or populated directly in photo-induced reactions due to the low transfer of angular momentum by photons. Therefore, the photoactivation process has to proceed indirectly via the resonant excitation of a higher-lying excited state, a so-called intermediate state (IS). Its decay subsequently can feed the isomeric or ground state, respectively, via electromagnetic transitions (γ transitions or internal conversion processes).

Unfortunately, there is a lack of monochromatic, tunable photon sources of high spectral intensity at MeV energies. However, the availability of high-current, low-energy electron accelerators can provide intense bremsstrahlung photon sources which can be used for improved photoactivation experiments [36].

The excitation energies and strengths of the IS can be extracted from bremsstrahlung-induced activation experiments by measuring the activation yields Y_{BS} as a function of the bremsstrahlung end point energy E_0. Since bremsstrahlung has a continuous energy distribution, the yields are given by the following integral:

$$Y_{BS}(E_0) \sim \int_0^{E_0} \sigma(E_\gamma) \cdot N_{BS}(E_0, E_\gamma) \cdot dE_\gamma, \qquad (1)$$

where $\sigma(E_\gamma)$ is the total photoreaction cross section as a function of the photon energy E_γ, corresponding to the energy E_{IS} of the intermediate state above the 75 keV isomer. The excitation energy E_x relative to the ground state of ^{180}Ta is given by $E_x = E_{IS} + 75$ keV. The quantity $N_{BS}(E_0, E_\gamma)$ represents the continuous bremsstrahlung spectral density with an end point energy E_0. The unquoted constant of proportionality is determined by the usual quantities such as target thickness, detector efficiencies, and the functions for the irradiation and counting times, respectively.

Low-energy, thick target bremsstrahlung spectra [39] show a nearly linear shape in the neighborhood of the end-point energy. This gives rise to an approximately linear yield

curve for one IS [40]. The onset of the yield curve is given by the excitation energy E_{IS} of the first IS. Each kink in the yield curve corresponds to the excitation energy of a further IS. The change of slope is proportional to the excitation strength of the respective IS (see, e.g., Ref. [41], and references therein).

In the following we summarize the relations needed for the description of the depopulation of a long-lived isomer by photoexcitation (the corresponding expressions for the population of isomers can be found elsewhere [36,40–42]). From the yield curve analysis the total detected activity I_D can be extracted, corresponding to the integrated cross section of the IS leading to a depopulation of the isomeric state,

$$I_D = g_{IS}\left(\frac{\pi\hbar c}{E_{IS}}\right)^2 \cdot \Gamma_{ISO} \cdot \frac{\Gamma_{\mathrm{g.s.}}}{\Gamma}. \tag{2}$$

Here, Γ_{ISO} denotes the partial decay width of the IS back to the isomeric state, $\Gamma_{\mathrm{g.s.}}$ stands for the total decay width of the IS to the short-lived ground state bypassing the isomeric state, and Γ is the total decay width of the IS. The spin factor g_{IS} takes into account the statistical weights of intermediate and isomeric states, respectively:

$$g_{IS} = \frac{2J_{IS}+1}{2J_{ISO}+1}. \tag{3}$$

Recent complementary investigations of both photoactivation with bremsstrahlung of variable end point energies *and* on-line nuclear resonance fluorescence experiments have demonstrated the reliability of modern photoactivation experiments and their analysis [36,43]. However, it should be emphasized that for a correct analysis of the yield curve all low-lying IS's have to be detected or known. Otherwise, the extracted cross sections are overestimated.

B. Photon scattering

Photon scattering nowadays represents an established technique in nuclear structure physics. In NRF experiments using continuous bremsstrahlung as a photon source and stable isotopes as targets all excited states with a sufficiently large ground-state decay width Γ_0 are excited simultaneously. Such experiments provide data concerning the following spectroscopic quantities: Precise excitation energies E_x can be extracted from the spectra of the scattered photons and the integrated scattering cross sections $I_{S,0}$ in the case of ground-state transitions are proportional to Γ_0^2/Γ. Therefore, the ground-state transition widths Γ_0 and the total widths Γ of the excited states can be extracted from the scattering intensities if all decay branchings are observed or known from other experiments. These quantities can be converted into reduced transition probabilities $B(E1)\uparrow, B(M1)\uparrow, B(E2)\uparrow$, or lifetimes $\tau=\hbar/\Gamma$. The formalism describing photon scattering experiments is summarized in previous reviews [44,45]. In the present case of photon scattering off a target nucleus in an isomeric state the integrated scattering cross section $I_{S,0}$ has to be replaced by the corresponding cross section $I_{S,ISO}$ and the widths Γ_0 by Γ_{ISO}, respectively.

C. Combined analysis of photoactivation and photon scattering experiments

Photoactivation and NRF experiments complement each other in an ideal way. The excitation energies and strengths of the IS can be determined directly and rather precisely, in on-line NRF experiments. However, the photoactivation technique offers some unique advantages for investigations of the depopulation or population of the isomers. The possible low-level, off-line detection of the activation yields and the higher available photon fluxes at irradiation facilities, as compared to the well-collimated narrow photon beams needed in photon scattering experiments, enables a considerably higher detection sensitivity.

Whereas in NRF experiments on nuclei existing in a long-lived isomer mainly excited states with a predominant decay to the isomeric state ($\Gamma_{ISO}/\Gamma \approx 1$) are observed, in photoactivation experiments IS's can be detected with decay branchings $\Gamma_{ISO}/\Gamma \ll 1$ which populate in a decay cascade the ground state bypassing the isomeric state. The new information obtained in this case is the effective branching ratio $\Gamma_{\mathrm{g.s.}}/\Gamma$. This branching ratio $\Gamma_{\mathrm{g.s.}}/\Gamma$ normally cannot be determined in NRF experiments. Therefore, photoactivation and photon scattering experiments are complementary spectroscopic methods. In the most favorable case where the intermediate state can be observed in both the photon scattering and photoactivation experiments, the ratio of the integrated cross sections directly provides the branching ratio $\Gamma_{\mathrm{g.s.}}/\Gamma_{ISO}$ without knowledge of the angular momentum J_{IS} and the total width Γ,

$$\frac{I_D}{I_{S,ISO}} = \frac{\Gamma_{\mathrm{g.s.}}}{\Gamma_{ISO}}. \tag{4}$$

D. Yield curve analysis

The yield curves measured in bremsstrahlung-induced reactions have to be transformed into the photonuclear cross sections or strength distributions of interest (in the case of bound states). These unfolding procedures have a long tradition in photonuclear physics (see, e.g., Ref. [46]). Nevertheless, since the unfolding in principle corresponds to a differentiation of the yield curve it is very difficult to avoid the generation and amplification of spurious structures and oscillations in the deduced cross sections even when applying sophisticated techniques such as variable energy binnings and smoothing procedures (see, e.g., Ref. [47]). A reliable unfolding represents a tough task already in the case of a rather smooth cross section curve, like giant resonances, but is even more difficult in the present case of discrete excitation strengths to bound states. The yield curves in the present experiments were taken in rather wide energy steps. In view of this limited number of data points and their scattering due to non-negligible systematic uncertainties the application of complete unfolding procedures seems to be inappropriate.

Therefore, a simple and more pragmatic analysis was applied to extract the integrated cross sections I_D.

The peak areas observed in the photon spectra of the off-line activation measurements were normalized for the corresponding irradiation and counting times. Low residual activities eventually existing from repeated irradiations of the sole enriched sample were properly corrected. The photon flux and the photon energy distribution were calculated for each end point energy by Monte Carlo simulations using the code GEANT 3.21. These calculations were experimentally checked by on-line NRF experiments and by simultaneous photoactivation measurements on ^{115}In [36]. From the onset of the activation the first IS was assumed at about 1.01 MeV above the isomer. In the following analysis the excitation energy of 1.01 MeV was used as a starting value for the analysis of the first part of the yield curve. In the first step of the analysis the data points up to the first kink in the yield curve were included. The energetic position of the lowest IS and its integrated depopulation cross section were then varied to deduce a best value for the cross section of the first IS from all yield points up to the first kink (see Fig. 5 below). By this, the integrated depopulation cross section I_D of the lowest IS could be determined. These values then are used for the next step in the data analysis where the yield points up to the second kink are taken into account. As a starting value the energetic position of the first kink is taken. Then the integrated cross section I_D is calculated for all yield data points up to the second kink subtracting the contribution of the lower-lying IS. Both the energetic position E_{IS} *and* the integrated cross section I_D are varied until the deduced cross sections are constant for all yield points considered. This analysis procedure was continued step by step from kink to kink of the yield curve over the whole energy range investigated in the present experiments (see Sec. IV C). It is clear from the analysis procedure that the values for the lower-lying IS's have a strong effect on the results for the higher-lying ones, leading to larger errors for both the energies E_{IS} and the cross sections I_D.

This analysis is very sensitive to the energetic position of the IS. For pronounced kinks a variation of only 20 keV leads to a much worse description of the measured yield points (reflected by an increase or decrease of the deduced integrated cross section). From this, the errors of the energies E_{IS} can be estimated and are quoted in Table I. These errors, depending on the changes of the slope of the yield curve, are comparable (20–60 keV) to the uncertainties for the absolute calibration of the bremsstrahlung endpoint energy of about 30 keV [36]. This type of analysis has been checked by applying it to measurements of the photoactivation of the ^{115}In^m isomer [36], where the energies and integrated cross sections of the IS's are known. The good agreement of the deduced results and those calculated from literature data [37] demonstrates the reliability of the applied analysis.

TABLE I. Intermediate states (IS's) observed in the photo-induced depopulation of ^{180}Ta^m. Given are the energies E_{IS} of the observed intermediate states (with respect to the isomer at 75 keV) with their uncertainties from the yield curve analysis (see text), the total integrated depopulation cross sections I_D, and the branching ratios $\Gamma_{ISO}\cdot\Gamma_{\mathrm{g.s.}}/\Gamma$ [see Eq. (2)]. For the cross sections and branching ratios, statistical and systematical errors are quoted separately (in this order).

E_{IS} (MeV)	I_D (eV b)			$g_{IS}\cdot\Gamma_{ISO}\cdot\Gamma_{\mathrm{g.s.}}/\Gamma$ (meV)		
1.01 [a]	0.057	±0.003	±0.015	0.015	±0.001	±0.004
1.22(2)	0.27	±0.02	±0.07	0.103	±0.008	±0.027
1.43(2)	0.24	±0.04	±0.06	0.126	±0.022	±0.033
1.55(3)	0.70	±0.09	±0.18	0.44	±0.06	±0.11
1.85(5)	1.11	±0.14	±0.29	1.0	±0.1	±0.3
2.16(2)	2.8	±0.3	±0.7	3.3	±0.3	±0.9
2.40(6)	3.5	±0.6	±0.9	5.2	±0.8	±1.4
2.64(3)	13	±1	±3	23	±2	±6
2.80(4)	36	±2	±9	73	±3	±19

[a]Fixed by the onset of the activation.

III. EXPERIMENTAL DETAILS

A. Irradiation facility

At the bremsstrahlung irradiation facility [36] installed recently at the Stuttgart DYNAMITRON accelerator, typical dc electron currents of 400–450 μA could be used on the water cooled bremsstrahlung production target in the whole energy range of interest (0.8 – 4 MeV). To achieve the highest possible photon flux the distance between the radiator target and the Ta samples to be activated was only about 9 cm. The samples could be transported to the activation location by a remotely controlled worm driven support. Details of the setup and the performed calibrations can be found in Ref. [36].

B. Ta targets

The availability of a highly precious Ta sample, representing the world's stock of enriched ^{180}Ta^m material, together with the new irradiation facility dramatically improved the sensitivity of the present study compared to older ones. In total about 150 mg of Ta_2O_5 material, enriched to 5.45% in ^{180}Ta^m, were available, corresponding to about 6.7 mg of ^{180}Ta^m. In view of the high price of the material, conventional target preparation methods like tablet pressing could not be applied since this technique is affected with appreciable material loss. Therefore, the Ta_2O_5 powder was packed into a graphite container consisting of a base and a cover. The target area was 1 cm^2, and the areal density amounted to 123 mg/cm^2 of Ta. The graphite container was fairly transparent for photons with energies of more than 50 keV. Therefore, the absorption of the Hf characteristic x rays by the graphite cover of the target was negligible. The target setup is described in more detail in Ref. [48].

Alternating with this sole enriched target assembly, foils of natural Ta metal (diameter 20 mm and total mass of Ta $\approx$1.5 g, corresponding to 0.18 mg of ^{180}Ta) were activated at bombarding energies above 1.7 MeV. In addition, a sample consisting of 150 mg natural Ta_2O_5, prepared in exactly the same way as the enriched target, was activated at higher bombarding energies around 3 MeV to verify the enrichment

factor. Typical irradiation and activation counting times were about two half-lives (12–20 h).

C. Photon detection system

After the irradiations characteristic x rays and nuclear γ rays from the activated samples were measured offline in a separate counting room using two well-shielded, high-resolution, low-energy photon (LEP) detectors facing each other [36]. The planar LEP crystals had a diameter of 52 mm and a sensitive volume of 42 cm^3. Background radiation was efficiently reduced by a sophisticated shield made of high-purity copper and lead. The excellent energy resolution of about 470 eV at 55 keV enabled the separation of the $K_{\alpha 1}$ (55.79 keV) and $K_{\alpha 2}$ (54.61 keV) characteristic x-ray lines of ^{180}Hf following the electron-capture decay of the ^{180}Ta ground state (see Fig. 1). The relative efficiencies of the detectors were determined using a ^{133}Ba γ source. At 59.5 keV the absolute efficiencies were measured by means of a calibrated ^{241}Am source. Total absolute efficiencies of about 20% and 28% at 55 keV could be achieved for both detectors, respectively. The estimated relative systematic uncertainties of these values are below 11%.

D. Photon scattering experiments

Supplementary photon scattering experiments were performed likewise at the bremsstrahlung facility of the Stuttgart accelerator [44]. The measurements were carried out at a bremsstrahlung end point energy of 1.5 MeV to achieve an optimal sensitivity at low excitation energies around 1 MeV where the lowest IS is assumed to lie. The dc electron currents used in the present experiments had to be limited, due to the thermal capacity of the radiator target, to values $\leqslant 420$ μA. The scattered photons were detected by three high-resolution Ge γ-ray spectrometers installed at angles of about 90°, 127°, and 150° with respect to the incoming bremsstrahlung beam. The efficiencies of all three detectors amounted to about 100% each, relative to a standard 7.6 cm$\times$7.6 cm NaI(Tl) detector. The energy resolution of all detectors was typically about 2 keV at a photon energy of 1.3 MeV. The Ge detector at 127° in addition was surrounded by a BGO anti-Compton shield [49] to improve its response function and hence to increase detection sensitivity.

In a first measurement, sheets of natural Ta metal were used as targets with a total mass of 1.797 g. A target of 1.011 g of LiF served as photon flux monitor. The total effective time of data collection in this measurement was 2 days. In a second run the enriched target sample of 150 mg Ta_2O_5 (enriched to 5.45% in $^{180}Ta^{m}$) together with the LiF material was bombarded for about 10 days at the same end-point energy of 1.5 MeV.

IV. RESULTS

A. Photon spectra of activated Ta samples

Figure 2 shows examples of the low-energy γ-ray and x-ray spectra of the enriched Ta sample from photoactivation

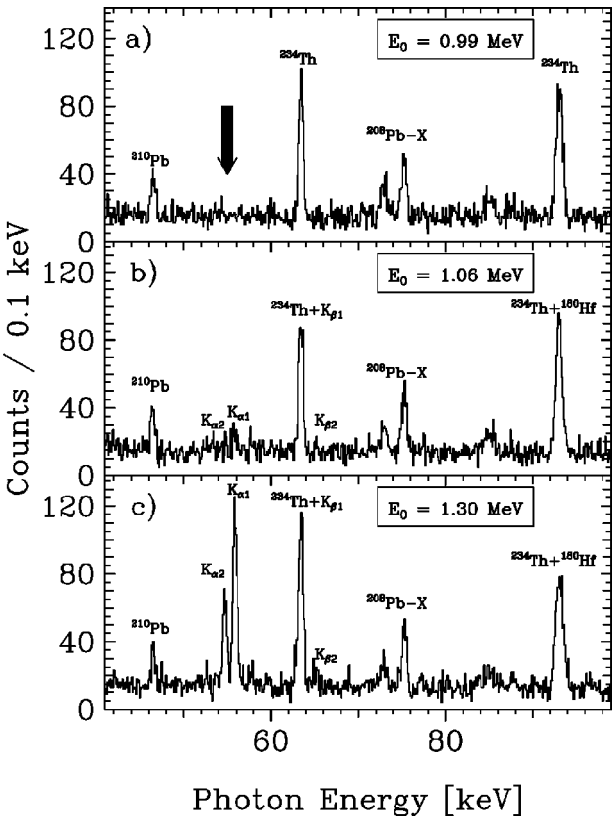

FIG. 2. Low-energy γ-ray and x-ray spectra of the enriched Ta sample from photoactivation at $E_0 = 0.99$, 1.06, and 1.30 MeV (a), (b), and (c). The Hf characteristic x rays are labeled by $K_{\alpha_{1,2}}$ and $K_{\beta_{1,2}}$. Background lines stemming from nuclear γ transitions in isotopes of natural decay chains or characteristic x rays are marked by the corresponding isotope symbols. In the top panel the energetic position of the Hf K_α lines is indicated by a bold arrow.

at the low bremsstrahlung end point energies of 0.99, 1.06, and 1.30 MeV. The Hf characteristic x rays of interest are labeled $K_{\alpha_{1,2}}$ and $K_{\beta_{1,2}}$. The origin of background lines is explained in the caption of Fig. 2.

The top panel shows the photon spectrum of the enriched target bombarded with bremsstrahlung of an end point energy $E_0 = 0.99$ MeV. Only background lines are visible. At the energetic position of the Hf K_α lines of interest, marked by an arrow, no peaks could be detected. The onset of the depopulation of the $^{180}Ta^{m}$ isomer has been observed starting at about $E_0 \geqslant 1.02$ MeV. In the middle panel, showing the spectra after an activation with $E_0 = 1.06$ MeV, the Hf characteric x rays could already be identified unambiguously. The spectrum taken after an activation at $E_0 = 1.30$ MeV is shown in the lowest panel and exhibits clearly the characteric x rays and nuclear γ transitions specific for the decay of the ground state of ^{180}Ta. The spectrum is dominated by the well-resolved K_{α_1} and K_{α_2} lines of Hf at 55.79 and 54.61 keV, respectively. The corresponding K_{β_1} and K_{β_2} peaks are also visible. Unfortunately, there are accidental overlaps of background lines (nuclear γ transitions following the β decay of ^{234}Th) with the K_{β_1} line and the $2^+ \rightarrow 0^+$ γ transi-

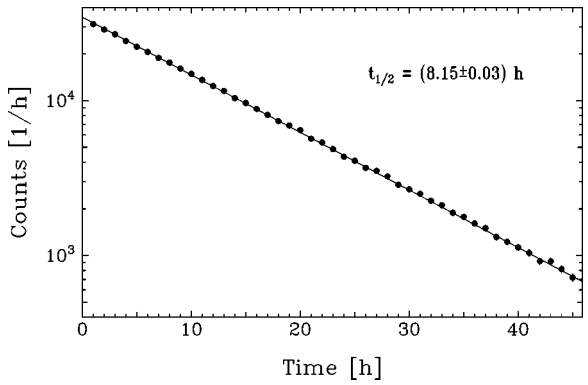

FIG. 3. Measured decay curve of the Hf K_α lines after photoactivation of the enriched Ta sample using bremsstrahlung with an end point energy of 3.1 MeV. The irradiation time was about 10 h. The statistical uncertainties of the data points are smaller than the symbol sizes.

tion in the residual nucleus ^{180}Hf, respectively. Therefore, the analysis was restricted to the K_α lines.

B. Half-life of the ^{180}Ta ground state

Additional proof for observing the ^{180}Ta ground-state decay is a confirmation of the lifetime in a time differential measurement. The results are depicted in Fig. 3. The enriched Ta sample was irradiated for about 10 h with bremsstrahlung of 3.1 MeV end point energy. The measurement of the activity covered about eight half-lives. The straight line represents a least squares fit to the data. The half-life could be determined from the slope rather precisely to $t_{1/2}^{exp} = (8.15 \pm 0.03)$ h, in good agreement with literature data [50].

To search for further possible short-lived isomers in ^{180}Ta two evaluation techniques were applied. First, a decay curve was generated from the list mode data with time binnings of 10 min. Covering the time range of the first 3.5 h no additional time component could be detected. As an alternative evaluation, the technique of using a compressed ^{2}log time scale [52] was applied. This method is known to be very sensitive to disentangle different time components in decay curves [52]. Also this analysis of the total data resulted in an excellent fit to the data [53] assuming only one half-life. The obtained value $t_{1/2} = 8.18(2)$ h was in perfect agreement with both the above-mentioned result of the traditional analysis and the best value given in the literature [50]. Therefore, the existence of further isomers with half-lives larger than a few minutes and essential contributions to the decay of the intermediate states can be excluded on the basis of the present experiments.

C. Activation yields and integrated depopulation cross sections

The relative yields, extracted from the peak areas of the ^{180}Hf K_α lines normalized to the number of incident electrons and to the irradiation and counting times, are plotted in Fig. 4 as a function of the bremsstrahlung end point energy.

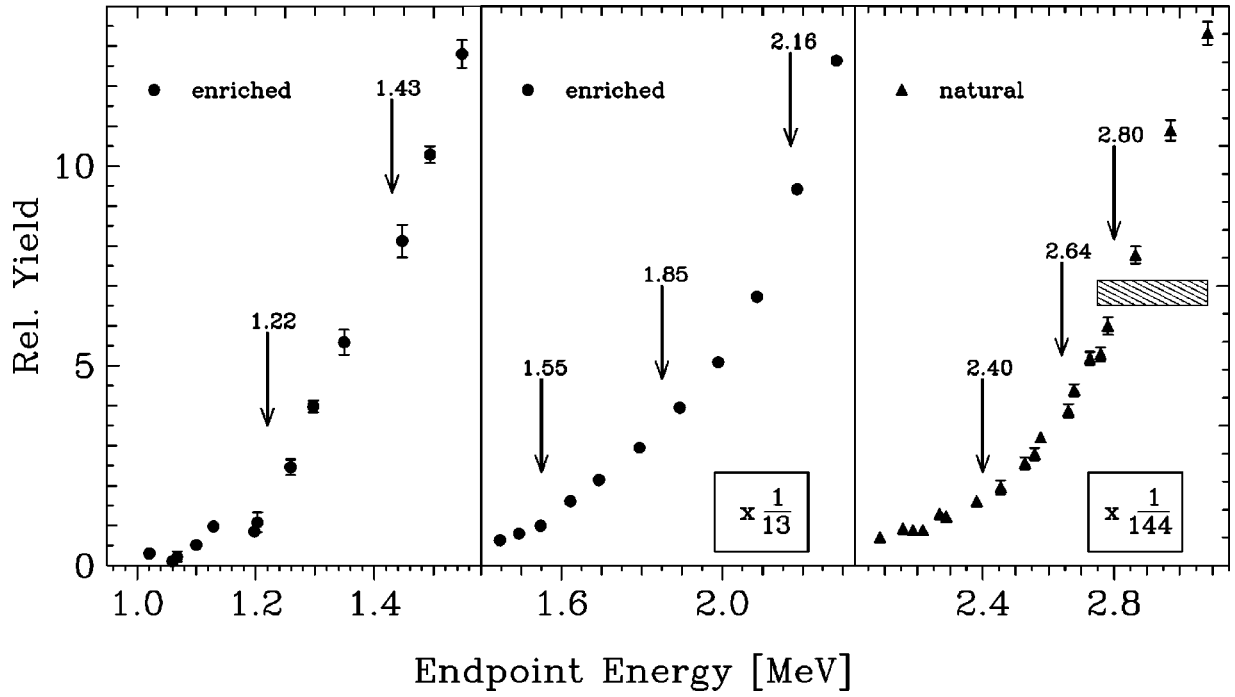

FIG. 4. Measured yields in a linear scale as a function of the end point energy. Shown are the peak areas of the Hf K_α lines, normalized to the number of incident electrons and the irradiation and measuring times (see text). Up to end point energies of 2.3 MeV (left and middle parts of the figure) the enriched sample was activated; for higher bombarding energies metallic natural Ta targets could be used (right part of the figure). The ordinate scales are properly changed to allow a clearly arranged linear presentation. The arrows mark the kinks in the yield curve caused by the different intermediate states. The hatched area in the right part of the figure represents the sensitivity limit reached in the experiments of Collins *et al.* (Ref. [19]).

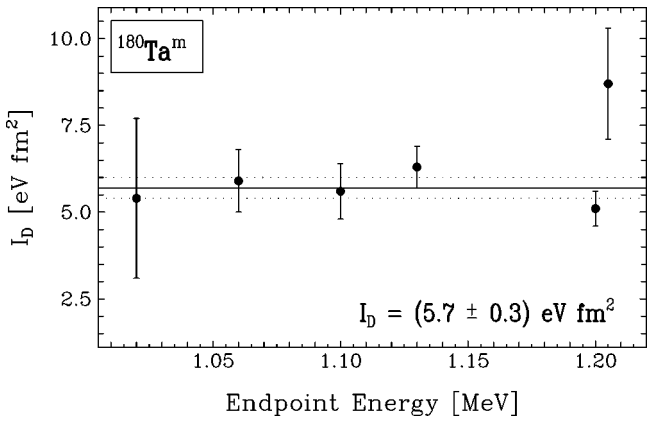

FIG. 5. Integrated depopulation cross section I_D of the first intermediate state (IS) according to the analysis of the lowest six yield data points, and assuming the energetic position of the first IS at $E_{IS}=1.01$ MeV above the isomer at 75 keV.

A linear scale for the ordinate was chosen for better visibility of the various kinks. Due to the large range of measured yields the figure is divided into three parts. The corresponding reduction factors for the scales in the middle and right part are given as insets. In the reduction factor of the right part the lower ^{180}Ta amount of a factor of 48 as compared to the enriched sample is taken into account. The low-energy activations were performed using the enriched target sample, while for end point energies above 2.3 MeV (right part) metallic sheets of natural Ta could be used. The arrows mark the kinks in the yield curve caused by the various IS's and the corresponding excitation energies E_{IS} are given in MeV.

The availability of the enriched target material, together with the new bremsstrahlung irradiation setup, has improved the sensitivity of the present study by a factor of about 4000 compared to previous experiments (Ref. [19], and references therein). For comparison, the sensitivity limit of the experiment by Collins *et al.* [19] is shown as a hatched area in the right part of Fig. 4.

The quantitative analysis of the yield curve, explained in Sec. II D, provided the numerical results summarized in Table I. Given are the excitation energies E_{IS} of the IS and the integrated depopulation cross sections I_D which can be expressed in terms of width ratios $g_{IS}\cdot\Gamma_{ISO}\cdot\Gamma_{\mathrm{g.s.}}/\Gamma$. The values for the energies E_{IS} and the integrated cross sections I_D were obtained from fits to the various linear sections of the yield curve. By way of example, the resulting best fit is shown in Fig. 5 for the data available to determine the lowest IS at 1.01 MeV photon energy.

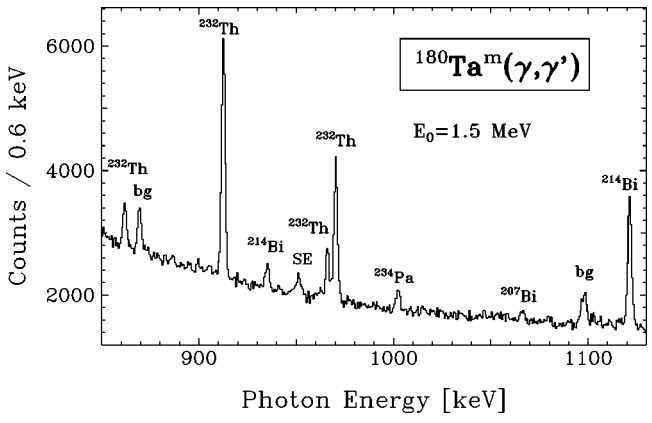

FIG. 6. Spectrum of photons scattered off the enriched $^{180}Ta^{m}$ sample using a bremsstrahlung beam of an end point energy of 1.5 MeV. Background transitions are marked. No peak which may be ascribed to transitions in ^{180}Ta or ^{181}Ta could be observed.

The given uncertainties of the excitation energies E_{IS} are estimated from the analysis of the yield curve (see Sec. II D). In addition, an overall uncertainty of the order of 30 keV exists due to systematic errors in the absolute calibration of the bremsstrahlung end point energies. The errors of the integrated cross sections are dominated by the systematical ones due to the necessary absolute calibrations. The relative error of the photon flux calibration amounts to about 10%, the uncertainties of the absolute efficiency determinations of the low-energy photon detectors to 11%. Furthermore, the relative intensities of the ^{180}Hf K_α lines (per g.s. decay of ^{180}Ta) are known with a relative precision of 5% only. It is obvious that the systematical errors of the integrated depopulation cross sections increase considerably for the higher-lying IS's due to unavoidable error propagation in the yield curve analysis. For these reasons statistical and systematical errors are quoted separately in Table I.

D. Results from photon scattering experiments

The first photon scattering experiments using natural Ta metallic targets, performed with bremsstrahlung of an end point energy of 1.5 MeV, failed to detect any excitation in ^{180}Ta. Obviously, the total amount of $^{180}Ta^{m}$ ($\approx$0.2 mg) contained in the natural sample was much too small. An estimate of the integrated scattering cross section of a hypothetical excitation at an excitation energy around 1 MeV provided a rather high detection limit of about $I_S \leqslant 80000$ eV b only. Therefore, in a subsequent photon scattering experiment the enriched sample, containing in total 6.7 mg of $^{180}Ta^{m}$, was used as a scattering target. Furthermore, the period of data collection was extended to 10 days.

Figure 6 shows the observed spectrum of scattered photons. The marked peaks correspond to known background γ rays. Unfortunately, none of the peaks observed could be ascribed to transitions in ^{180}Ta. Surprisingly, also no low-energy transitions in ^{181}Ta, which made up 95% of the Ta sample, could be detected. Obviously, there is a lack of dipole strength at low energies and the stronger dipole excitations in ^{181}Ta are concentrated at higher excitation energies of about 2.3 and 3.0 MeV, as observed in previous photon scattering experiments off ^{181}Ta [51]. The sensitivity limit in the present photon scattering experiments was estimated from the statistics of the continuous background distribution. Requiring a peak area larger than a 2σ deviation of the corresponding background counts, no excitation in the most interesting energy range around 1 MeV could be detected with an integrated scattering cross section of $I_S \geqslant 200$ eV b. This limit is about a factor of 400 lower than that derived from the experiment using the metallic natural Ta sheets. Nevertheless, it is still four orders of magnitude larger than the g.s.

decay branch observed in the photoactivation experiment.

V. DISCUSSION

A. Comparison with previous investigations

Previous measurements of ^{180}Ta excitation functions by photoactivation with bremsstrahlung have been reported in Refs. [19,54]. In Ref. [19] an onset of ^{180}Ta g.s. decay was observed at an end point energy of about 2.8 MeV and IS's at 2.8(1) and 3.6(1) MeV were deduced. Because of the coarse energy steps of the excitation function the lower IS might correspond to the intermediate levels at $E_{IS}=2.64$ and 2.80 MeV from the present work. For comparison of the integrated cross sections with the value given in Ref. [19] the contributions of lower-lying IS's, observed for the first time in the present experiment, must be subtracted. After the correction an integrated cross section of 58(17) eV b is found, about 50% higher than in the present work but still within statistical and systematical uncertainties of both the present data and that of Ref. [19]. Karamian *et al.* [54] extended the measurements of the $^{180}\mathrm{Ta}^m(\gamma,\gamma')$ reaction up to $E_0=7.6$ MeV and deduced the g.s. population branching ratio as a function of E_0.

Isomer depopulation by strong radioactive ^{60}Co sources has also been searched for [20–22]. Only in Ref. [22] was a weak positive signal observed. However, subsequent measurements with an improved detection setup confirmed the result with much better statistics [55]. Because the photon flux was determined using ^{115}In as a reference (see Ref. [36]), the measured yield can be converted to an integrated cross section for an excitation energy close to the dominant IS in ^{115}In at $E_x=1.078$ MeV resulting in $I_D=0.13(4)$ eV b. The larger I_D value with respect to the lowest IS found in the present work (cf. Table I) can be understood from the additional contribution of the next-higher IS at $E_{IS}=1.22$ MeV. With reasonable assumptions about the photon flux at the higher energy the findings of Refs. [22,55] are in agreement with the results presented in Table I.

A comparison of the photoexcitation results to those of Coulomb excitation experiments is less straightforward. In general, Coulomb excitation functions are less sensitive to the excitation energy of the IS and contributions of several IS's cannot be decomposed. However, because of the strong excitation energy dependence of the Coulomb excitation cross section it is reasonable to assume that only a single IS (lowest in energy) is responsible for the observed yield. The ^{32,36}S induced experiments of Schlegel *et al.* [23] indicated $E_{IS}\leqslant 1$ MeV, but the Hf *K* x-ray signal was hampered by a strong Ta x-ray signal resulting from β decay produced in background reactions. Depopulation of the isomer was also observed in light-ion induced Coulomb excitation, but the data suggested a significantly higher energy at $E_{IS}\approx 2.2$ MeV [24]. Recent experiments using ^{36}S and ^{64}Ni beams and enriched targets find a clear signal compatible with an IS at $E_{IS}\simeq 1.08(4)$ MeV [25,56]. One should note the different selectivity of Coulomb excitation where $E2$ and $E3$ transitions are favored. This might explain the nonobservation of the lowest IS. For example, assuming an $M1$ transition Coulomb excitation would be negligible.

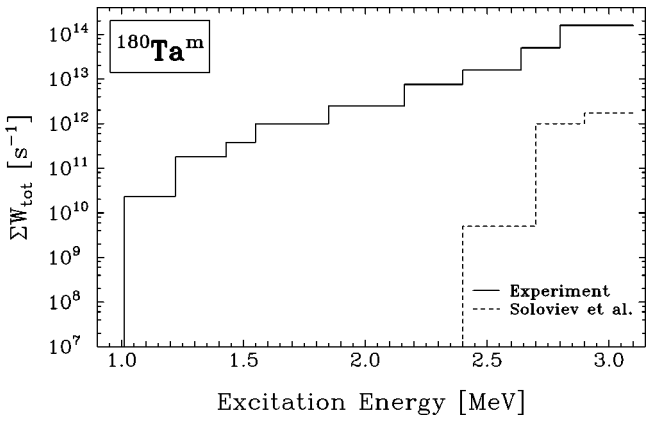

FIG. 7. Summed experimentally determined transition rates ΣW_{tot} (full line) in comparison with the results of the calculations by Soloviev *et al.* (Refs. [57,58]), see the hatched line.

B. Comparison with theoretical calculations

The theoretical description of heavy odd-odd nuclei is particularly difficult due to the complicated interplay of single-particle and collective degrees of freedom. Nevertheless, Soloviev [57] has studied the excitation spectrum of collective vibrations built on the $J^\pi=9^-$ and $J^\pi=16^+$ high-spin isomers in ^{180}Ta and ^{178}Hf, respectively, in the framework of the quasiparticle-phonon model (QPM) in a deformed single-particle basis. Recently, also the photodeexcitation process of $^{180}\mathrm{Ta}^m$ was treated by extending the model space to include collective excitations built on the g.s. and a calculation of all possible transitions between these groups of states [58].

The transition rate W for one excited state is given by

$$W=\frac{8\pi}{\hbar}\sum_{\pi L}\frac{L+1}{L[(2L+1)!!]^2}\cdot\left(\frac{E_\gamma}{\hbar c}\right)^{2L+1}\cdot B(\pi L). \quad (5)$$

For the multipolarities relevant for photon scattering this leads to

$$W(E1)=1.59\times 10^{15}E_\gamma^3\cdot B(E1)\uparrow, \quad (6)$$

$$W(E2)=1.22\times 10^{9}E_\gamma^5\cdot B(E2)\uparrow,$$

$$W(M1)=1.76\times 10^{13}E_\gamma^3\cdot B(M1)\uparrow,$$

where W is in units of 1/s, E_γ is in MeV, and the reduced transition probabilities are in $e^2\,\mathrm{fm}^{2L}$ for electric and in μ_N^2 for magnetic transitions.

The total transition rate W_{tot} for the two-step process of the excitation of an IS and its decay to the vibrational states built on the ground state can be calculated from the experimentally measured integrated cross section I_D using Eq. (2),

$$W_{tot}=1.52\times 10^{15}\cdot I_D\cdot\left(\frac{E_\gamma}{\pi\hbar c}\right)^2, \quad (7)$$

where I_D is in units of eV fm^2.

For comparison of the experimental data with the QPM calculations [58], the hatched line in Fig. 7, the total transi-

tion rate ΣW_{tot} summed over the contributions of all IS's up to a certain excitation energy was calculated. The results are plotted in Fig. 7 as a solid line.

Below $E_x = 2.7$ MeV the QPM calculations find very little coupling between isomer and ground state. A sudden onset is observed around 2.7 MeV related to the decisive role of two-phonon excitations. These strong contributions are theoretically explained as a three-step process: In the first step, IS's are excited by fast dipole transitions through one-phonon components of the wave functions of the vibrational states built on the isomer, while the second step is dominated by collective $E2$ transitions from two-phonon components of these states to the one-phonon vibrational states built on the ground state. The third step is a complicated γ cascade from the vibrational states to the ^{180}Ta ground state.

However, even at higher energies, where significant transition rates are calculated in Ref. [58], the data are underpredicted by about two orders of magnitude. One possible explanation for this shortcoming could be the assumption of K symmetry. This may approximately hold for energies below $E_x \simeq 1$ MeV, but at higher excitation energies K mixing might be expected to increase the transition rates considerably. A dramatic reduction of K hindrance factors has been observed for multi-quasi-particle isomers in the $A = 180$ mass region (see, e.g., Ref. [59]) and complete K mixing near the neutron binding energy has been observed [54]. The systematics reveal a striking dependence on the energy relative to the yrast level indicating statistical mixing as the most important source [60]. For excitation energies of more than 2.5 MeV above the yrast line (note that the isomer in ^{180}Ta is the 9^- yrast state) these results suggest that K hindrance plays a limited role only.

Another QPM calculation for ^{180}Ta has been performed by Alexa *et al.* [61] limited to lower excitation energies but including Coriolis mixing. Because of the latter, some IS candidates appear below 1.5 MeV, but the transition rates are again much smaller than found experimentally.

C. Astrophysical implications: the nucleosynthesis of $^{180}Ta^m$

As pointed out in the introduction, the nucleosynthesis of $^{180}Ta^m$ is a yet unsolved problem. The production mechanism is not clear but possible paths have been predicted for the *s* process [8], the ν process [62], and the *p* process [63]. The relevance of the present work lies in the experimental information on an electromagnetic coupling between the long-lived isomer and the short-lived ground state. Depending on the temperature of the stellar environment, the photon bath present during the different processes may effectively depopulate the isomer and destroy parts or all of synthesized $^{180}Ta^m$.

1. s-process considerations

The role of the isomer depopulation in *s*-process scenarios has been discussed in detail in Ref. [38]. Therefore, we restrict ourselves here to one particular aspect. The present results largely exclude *s*-process production of $^{180}Ta^m$ with typical temperatures deduced from branching points in the canonical model [5]. However, within the most advanced dynamical models [64] freshly synthesized ^{180}Ta can survive because of strong convection with a time scale still shorter than the effective lifetime at maximum *s*-process temperatures of about 3×10^8 K. At these temperatures the effective lifetime is almost exclusively determined by the energy of the lowest IS. It must be noted that the available data do not permit to distinguish whether the onset of isomer depopulation at $E_{IS} \simeq 1$ MeV is due to the lowest IS or due to reaching the sensitivity limit of the experiment. The yield data (Fig. 4) could alternatively be interpreted as arising from an IS at even lower energy with correspondingly smaller integrated cross sections.

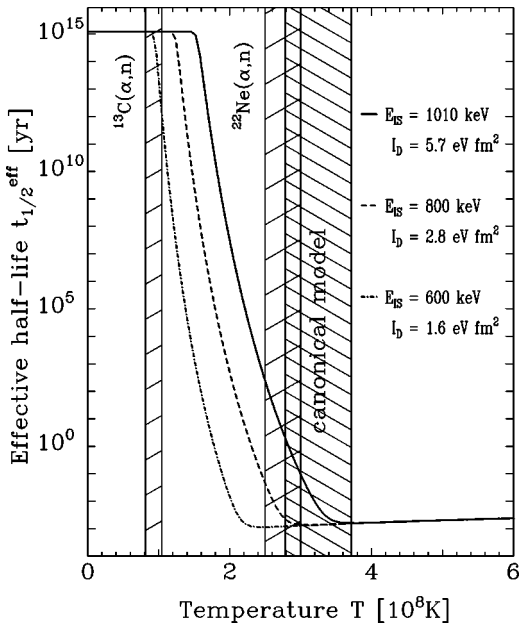

FIG. 8. Reduction of the $^{180}Ta^m$ effective half-life in the presence of a stellar photon bath deduced from the photoactivation cross sections measured in the present experiments assuming the lowest IS at excitation energies of 1.01, 0.8, and 0.6 MeV above the isomer, respectively. Thermal energy ranges expected under *s*-process conditions are indicated (\\\) for the canonical model (Ref. [5]) and for a more realistic model (Ref. [64]) which distinguishes burning phases (///) where different (α,n) reactions serve as neutron sources, see text.

The impact of such an assumption is demonstrated in Fig. 8. The effective half-life is shown as a function of the photon bath temperature for the properties of the lowest IS (at $E_{IS} = 1.01$ MeV) deduced from the data and assuming lower energies $E_{IS} = 800$ and 600 keV with I_D corrected to account for the measured yields. The typical temperature regimes of the canonical and dynamical *s*-process models are shown as hatched areas. Even at the lower temperatures assumed in the dynamical model, for ^{22}Ne(α,n) induced synthesis the effective half-life of ^{180}Ta would be reduced to the g.s. half-life for $E_{IS} \approx 700$ keV precluding any production. Note that the burning phases with neutron production by the ^{13}C(α,n) reaction do not contribute to the ^{180}Ta synthesis because the temperature is too low to induce β decay from excited states in ^{179}Hf [8].

Due to the strong energy dependence new experimental efforts to lower the sensitivity threshold would be of considerable importance.

2. Neutrino nucleosynthesis

As an alternative astrophysical site for the production of ^{180}Ta Woosley *et al.* proposed the neutrino nucleosynthesis in a type II supernova [62]. As the newly born neutron star remnant cools mainly by neutrino-pair production with approximately equal luminosities for all three neutrino flavors, the outer shells of the star are subjected to immensely high fluxes of neutrinos. For the neutrino nucleosynthesis neutral-current reactions by ν_x neutrinos (customarily used for supernova ν_μ and ν_τ neutrinos and their antiparticles which all have quite similar distributions) are of special interest as they have noticeably larger average energies ($\langle E_{\nu_x}\rangle \sim 25$ MeV) than supernova ν_e and $\bar{\nu}_e$ neutrinos ($\langle E_{\nu_e}\rangle \sim 12$ MeV, $\langle E_{\bar{\nu}_e}\rangle \sim 16$ MeV, see Ref. [65]). Inelastic scattering by ν_x neutrinos dominantly excites nuclei to levels above particle thresholds. The subsequent nuclear decays, mainly by proton or neutron emission, contribute to the element synthesis of the daughter nuclides. It has been observed that supernova neutrino nucleosynthesis can become a significant production process for the daughter nuclide if one wants to explain abundance ratios of parent to daughter which exceed about 10^3 [66]. In that case a ppm (or less) neutrino spallation of the parent is sufficient to explain the abundance of the daughter. Obviously the process does not affect the parent abundance.

One such pair of nuclides is ^{181}Ta and ^{180}Ta with an observed abundance ratio of $R = {}^{180}\mathrm{Ta}/{}^{181}\mathrm{Ta} = 1.2\times 10^{-4}$. Woosley *et al.* proposed that ^{180}Ta can be made by $(\nu_x, \nu_x' n)$ reactions on preexisting ^{181}Ta [62]. As the actual site for the ^{180}Ta production, these authors identified the neon burning shell, which is also the site of the *p* (or gamma) process, where explosive burning leads to photodisintegration of nuclei existing in these mass zones from prior burning during stellar evolution. At larger stellar radii, the inelastic scattering rate, which, due to its dependence on the neutrino flux, scales inversely with the square of the radius, is too small while at smaller radii, the produced ^{180}Ta is destroyed by photodissociation when the shock wave passes subsequently through the neon shell and heats the matter to a few 10^9 K. In their nucleosynthesis calculations Woosley *et al.* find an overproduction rate of the ^{180}Ta/^{181}Ta abundance ratio in massive stars which would be sufficient to explain the observed abundance of ^{180}Ta. This study, however, has been based on a rather crude estimate of the total inelastic neutrino scattering cross section on ^{181}Ta which was obtained from the estimate of the ^{56}Fe cross section by scaling with the ratio of mass numbers [62]. This estimate is likely too large for at least two reasons: (i) While calculations reveal that the total inelastic neutrino scattering cross section for supernova ν_x neutrinos indeed scales approximately with the mass number, it is the partial $^{181}\mathrm{Ta}(\nu_x, \nu_x' n)$ cross section which matters for the neutrino nucleosynthesis of ^{180}Ta. This partial cross section is noticeably smaller than the total cross section as most of the Gamow-Teller excitations are below the neutron threshold in ^{181}Ta ($E_n \sim 7.6$ MeV), while part of the forbidden strength is expected to be located above the two-nucleon threshold $E_{2n} \sim 17.9$ MeV. (ii) After neutrino nucleosynthesis and passage of the shock wave only a fraction of the ^{180}Ta will be in the isomeric state and will thus survive.

Recalling the strong sensitivity of the ^{180}Ta *s*-process abundance on details of the astrophysical *s* process and hence its potential importance as a constraint for the site and dynamics of the process, it is obviously quite relevant to determine how much ^{180}Ta can be produced by alternative astrophysical sites, e.g., by neutrino nucleosynthesis. For that reason we have performed a detailed calculation of the $^{181}\mathrm{Ta}(\nu_x, \nu_x' n)$ cross section. We assume a two-step process. In the first step the $^{181}\mathrm{Ta}(\nu_x, \nu_x')^{181}\mathrm{Ta}^*$ cross section is calculated as a function of excitation energy in ^{181}Ta within the random phase approximation. The ^{181}Ta ground state is described in the spherical approximation assuming equal fillings of all *m* states in the valence shell. This approximation is reasonable as the ν_x neutrinos mainly excite collective modes which are not too sensitive to detailed nuclear structure [67]. Details of the model and the adopted formalism can be found in Refs. [68,69]. As residual interaction a zero-range Landau-Migdal interaction is chosen. For the supernova ν_x neutrinos a Fermi-Dirac spectrum with temperature $T = 8$ MeV and zero chemical potential is adopted. These neutrinos are already energetic enough that the dependence of the multipole operators on the momentum transfer has to be taken into account. Here, we follow the formalism derived in Ref. [70] and consider multipole excitations with spin up to $J = 4$ and both parities.

In the second step for each final state with well-defined energy the branching ratios into the various decay channels are calculated using the statistical model code smoker [71]. Possible final states in the residual nucleus considered by the smoker code are experimentally known levels supplemented at higher energies by an appropriate level density formula [71]. As decay channels the code considers proton, neutron, and α and γ emissions. If the decay leads to an excited level of the residual nucleus (e.g., to $n + {}^{180}\mathrm{Ta}^*$), we calculate the branching ratios for the decay of this state in an analogous fashion. Keeping track of the energies of the ejected particles and photons during the cascade, and weighting them with appropriate branching ratios and the corresponding $^{181}\mathrm{Ta}(\nu, \nu')^{181}\mathrm{Ta}^*$ cross section, the various partial particle and photon spectra are determined. The branching ratios are found to be quite insensitive to the spin assignments of the decaying states. This allows us to sum over the different multipole contributions before multiplying with the branching ratios.

A total inelastic cross section for supernova ν_x scattering off ^{181}Ta of 144×10^{-42} cm^2 is deduced. Note that this cross section per nucleon is very close to the ^{56}Fe cross section per nucleon, given in Ref. [72]. About 37% of the cross section lies below the neutron threshold, corresponding mainly to Gamow-Teller excitations. The excited states decay by gamma emission back to the ^{181}Ta ground state and thus do not contribute to the ^{180}Ta production. The excited states

above the neutron threshold decay by neutron emission, as the large Coulomb barriers severely suppress decay into the proton and α channels. However, in about one third of the cases the neutron emission populates the daughter nucleus ^{180}Ta in an excited state above its respective neutron threshold. Thus, these states decay again by neutron emission, leading to states in ^{179}Ta and hence also do not contribute to the ^{180}Ta production. We thus find a partial $^{181}\mathrm{Ta}(\nu_x,\nu_x' n)$ cross section of 57×10^{-42} cm^2 for reactions which lead to particle-bound states in ^{180}Ta and will end up either in the ground state or in the long-lived isomer. Our cross section is smaller than the one used by Woosley *et al.* by a factor of 4.2. The lifetimes of both states are long compared to the time which proceeds between neutrino nucleosynthesis in the neon shell and arrival of the supernova shock wave. The shock wave will heat the matter to temperatures in excess of 10^9 K which is hot enough to bring the ground state and the isomeric state into thermal equilibrium. Neglecting freeze-out effects and assuming a temperature of $T\sim10^9$ K leads to about 73% population of the produced ^{180}Ta nuclei in the isomeric state.

Inserting these cross sections into the model of Ref. [62], the net production rate of ^{180}Ta by neutrino nucleosynthesis is about a factor of 6 smaller. The resulting overproduction rate for the $^{180}\mathrm{Ta}/^{181}$Ta abundance ratio makes neutrino nucleosynthesis still a potential ^{180}Ta production site. It would be quite welcome if this crude estimate is followed up by detailed nucleosynthesis calculations using the improved neutrino cross sections. Finally we remark that production of ^{180}Ta by charged-current reactions on ^{180}W or ^{180}Hf is rather unimportant since for the $\overline{\nu}_e$-induced reaction on ^{180}Hf the cross section is strongly reduced due to the appreciable neutron excess, while the (ν_e,e^-) reaction on ^{180}W does not contribute since the ^{180}W abundance is two orders of magnitude smaller than the ^{181}Ta abundance.

3. p-process nucleosynthesis

As yet another alternative to the *s* process, a *p*-process origin of ^{180}Ta has been proposed [63]. Because of a delicate balance between ^{180}Ta production and destruction by (γ,n) reactions it works only in a constrained temperature window around $T=2\times10^9$ K [73] and is therefore strongly dependent on the underlying model. Because of the higher temperatures with respect to the *s* process, higher-lying IS's may be important for the effective half-life. This has to be implemented in further analyses of the *p*-process nucleosynthesis of ^{180}Ta.

VI. SUMMARY AND OUTLOOK

The present work provides a comprehensive study of the depopulation of the long-lived isomer $^{180}Ta^{m}$ by resonant photoabsorption for bremsstrahlung end point energies below 3 MeV. With the improved experimental setup and the use of the world's stock of isotopically enriched ^{180}Ta material an unprecedented sensitivity could be reached. This allowed the identification of IS's with sizable integrated cross sections down to excitation energies of about 1 MeV.

With reasonable assumptions on the branching ratio of IS's between decay to the g.s. and back decay to the isomer one finds rather large electromagnetic transition probabilities typical of unhindered transitions. This implies considerable *K* mixing already at low energies. Theoretical interpretations of this phenomenon are presently missing. Microscopic QPM calculations, while providing a satisfactory description of collective excitations built on the isomer, underpredict the g.s. decay by about 2 to 3 orders of magnitude.

The astrophysical implications of the present results for explosive production scenarios need further exploration. Experimentally, new measurements with improved experimental limits would be of high importance to provide a final answer to the still open possibility of an *s*-process synthesis of $^{180}Ta^{m}$.

Finally, the combination of NRF and photoactivation techniques at the new facility at Stuttgart certainly represents an important step for further studies on nuclear structure as well as astrophysical problems. An interesting application for the latter could be ^{176}Lu which has been shown to be a thermometer of the *s* process due to the occurrence of a low-lying IS [74,75].

ACKNOWLEDGMENTS

The authors wish to thank G. Sletten and C. Günther for lending the LEP detectors used in the experiments. We are grateful to N. Auerbach, G.D. Dracoulis, E.B. Norman, T. Rauscher, G. Sletten, the late V.G. Soloviev, S.E. Woosley, and L. Zamick for enlightening discussions. The support by the Deutsche Forschungsgemeinschaft under Contract Nos. Kn 154/30 and FOR 272/2-1, the BMBF under Contract No. 06DA915I, the Munich Tandem Accelerator Laboratory, the FZ Karlsruhe, and by the U.S. AFOSR under Contract No. F49020-99-1-0263 is gratefully acknowledged.

[1] N. Boos, F. Le Blanc, M. Krieg, J. Pinard, G. Huber, M. D. Lunney, D. Le Du, R. Meunier, M. Hussonnois, O. Constantinescu, J. B. Kim, Ch. Briançon, J. E. Crawford, H. T. Duong, Y. P. Gangrski, T. Kuhl, B. N. Markov, Yu. Ts. Oganessian, P. Quentin, B. Roussiere, and J. Sauvage, Phys. Rev. Lett. **72**, 2689 (1994).

[2] S. Deylitz, B. D. Valnion, K. El Abiary, J. de Boer, N. Gollwitzer, R. Hertenberger, G. Graw, R. Kulessa, Ch. Briançon, D. Le Du, R. Meunier, M. Hussonnois, O. Constantinescu, S. Fortier, J. B. Kim, L. H. Rosier, G. Rotbard, Yu. Ts. Oganessian, S. A. Karamian, H. J. Wollersheim, H. Folger, J. Gerl, Th. Happ, and C. Hategan, Phys. Rev. C **53**, 1266 (1996).

[3] E. Lubkiewicz, H. J. Wollersheim, R. Kulessa, Ch. Briançon, W. Brüchle, O. Constantinescu, M. Debowski, E. Ditzel, H. Folger, J. Gerl, F. Hannachi, T. Happ, M. Hussonnois, E. Jäger, S. Karamian, M. Kaspar, Th. Kröll, Yu. Ts. Oganessian, I. Pe-

ter, H. Schaffner, S. Schremmer, R. Schubert, N. Trautmann, K. Vetter, and G. Zauner, Z. Phys. A **355**, 377 (1996).
[4] T. Morikawa, Y. Gono, K. Morita, T. Kishida, T. Murakami, E. Ideguchi, H. Kumagai, G. H. Liu, A. Ferragut, A. Yoshida, Y. H. Zhang, M. Oshima, M. Sugawara, H. Kusakari, M. Ogawa, M. Nakajima, H. Tsuchida, S. Mitarai, A. Odahara, M. Kidera, M. Shibata, J. C. Kim, S. J. Chae, Y. Hatsukawa, and M. Ishihara, Phys. Lett. B **350**, 169 (1995).
[5] F. Käppeler, Prog. Part. Nucl. Phys. **43**, 419 (1999).
[6] H. Beer and R. A. Ward, Nature (London) **291**, 308 (1981).
[7] S. E. Kellogg and E. B. Norman, Phys. Rev. C **46**, 1115 (1992).
[8] K. Yokoi and K. Takahashi, Nature (London) **305**, 198 (1983).
[9] M. Schumann and F. Käppeler, Phys. Rev. C **60**, 025802 (1999).
[10] K. Wisshak, F. Voss, C. Arlandini, F. Bečvář, O. Straniero, R. Gallino, M. Heil, F. Käppeler, M. Krtička, S. Masera, R. Reifarth, and C. Travaglio, Phys. Rev. Lett. **87**, 251102 (2001).
[11] C. B. Collins and J. J. Carroll, Hyperfine Interact. **107**, 3 (1997).
[12] F. Stedile, E. Fill, D. Belic, P. von Brentano, C. Fransen, A. Gade, U. Kneissl, C. Kohstall, A. Linnemann, P. Matschinsky, A. Nord, N. Pietralla, H. H. Pitz, M. Scheck, and V. Werner, Phys. Rev. C **63**, 024320 (2001).
[13] S. Olariu and A. Olariu, Phys. Rev. Lett. **84**, 2541 (2000).
[14] D. P. McNabb, J. D. Anderson, J. A. Becker, and M. S. Weiss, Phys. Rev. Lett. **84**, 2542 (2000).
[15] P. von Neumann-Cosel and A. Richter, Phys. Rev. Lett. **84**, 2543 (2000).
[16] C. B. Collins, F. Davanloo, M. C. Iosif, R. Dussart, J. M. Hicks, S. A. Karamian, C. A. Ur, I. I. Popescu, V. I. Kirischuk, J. J. Carroll, H. E. Roberts, P. McDaniel, and C. E. Crist, Phys. Rev. Lett. **82**, 695 (1999).
[17] I. Ahmad, J. C. Banar, J. A. Becker, D. S. Gemmell, A. Kraemer, A. Mashayeki, D. P. McNabb, G. G. Miller, E. F. Moore, L. N. Pangault, R. S. Rundberg, J. P. Schiffer, S. D. Shastri, T. F. Wang, and J. B. Wilhelmy, Phys. Rev. Lett. **87**, 072503 (2001).
[18] J. J. Carroll, J. A. Anderson, J. W. Glesener, C. D. Eberhard, and C. B. Collins, Astrophys. J. **344**, 454 (1989).
[19] C. B. Collins, J. J. Carroll, T. W. Sinor, M. J. Byrd, D. G. Richmond, K. N. Taylor, M. Huber, N. Huxel, P. von Neumann-Cosel, A. Richter, C. Spieler, and W. Ziegler, Phys. Rev. C **42**, R1813 (1990).
[20] Zs. Németh, F. Käppeler, and G. Reffo, Astrophys. J. **392**, 277 (1992).
[21] E. B. Norman, S. E. Kellogg, T. Bertram, S. Gil, and P. Wong, Astrophys. J. **281**, 381 (1984).
[22] I. Bikit, L. Lakosi, J. Sáfár, and Lj. Čonkić, Astrophys. J. **522**, 419 (1999).
[23] C. Schlegel, P. von Neumann-Cosel, F. Neumeyer, A. Richter, S. Strauch, J. de Boer, C. H. Dasso, and R. J. Peterson, Phys. Rev. C **50**, 2198 (1994).
[24] M. Schumann, F. Käppeler, R. Böttger, and H. Schölermann, Phys. Rev. C **58**, 1790 (1998).
[25] M. Loewe, J. Besserer, J. de Boer, H. J. Maier, M. Würkner, J. Srebrny, T. Czosnyka, J. Iwanicki, P. J. Napiorkowski, P. von Neumann-Cosel, A. Richter, C. Schlegel, H. J. Wollersheim, P. Alexa, A. I. Levon, S. A. Karamian, and G. Sletten, Acta Phys. Pol. B **30**, 1319 (1999); (private communication).
[26] G. D. Dracoulis, F. G. Kondev, A. P. Byrne, T. Kibedi, S. Bayer, P. M. Davidson, P. M. Walker, C. Purry, and C. J. Pearson, Phys. Rev. C **53**, 1205 (1996).
[27] G. D. Dracoulis, S. M. Mullins, A. P. Byrne, F. G. Kondev, T. Kibedi, S. Bayer, G. J. Lane, T. R. McGoran, and P. M. Davidson, Phys. Rev. C **58**, 1444 (1998).
[28] T. R. Saitoh, N. Hashimoto, G. Sletten, R. A. Bark, S. Tormanen, M. Bergstrom, K. Furuno, K. Furutaka, G. B. Hagemann, T. Hayakawa, T. Komatsubara, A. Maj, S. Mitarai, M. Oshima, J. Sampson, T. Shizuma, and P. G. Varmette, Nucl. Phys. **A660**, 121 (1999).
[29] G. D. Dracoulis, T. Kibedi, A. P. Byrne, R. A. Bark, and A. M. Baxter, Phys. Rev. C **62**, 037301 (2000).
[30] C. Wheldon, P. M. Walker, P. Chowdhury, I. Shestakova, R. D'Alarcao, I. Ahmad, M. P. Carpenter, D. M. Cullen, R. V. F. Janssens, T. L. Khoo, F. G. Kondev, C. J. Lister, C. J. Pearson, Zs. Podolyak, D. Seweryniak, and I. Wiedenhoever, Phys. Rev. C **62**, 057301 (2000).
[31] E. B. Norman (private communication).
[32] C. Günther (private communication).
[33] P. M. Walker, G. D. Dracoulis, and J. J. Carroll, Phys. Rev. C **64**, 061302(R) (2001).
[34] M. Loewe, J. de Boer, H. J. Maier, M. Würkner, P. Olbratowski, J. Srebrny, J. Choinski, T. Czosnyka, J. Iwanicki, P. J. Napiorkowski, G. Hagemann, G. Sletten, S. A. Karamnian, P. von Neumann-Cosel, A. Richter, C. Schlegel, and H. J. Wollersheim, Z. Phys. A **356**, 9 (1996).
[35] C. Schlegel, P. von Neumann-Cosel, J. de Boer, J. Gerl, M. Kaspar, I. Kozhoukharov, M. Loewe, H. J. Maier, P. J. Napiorkowsky, I. Peter, M. Rejmund, A. Richter, H. Schaffner, J. Srebrny, M. Würkner, and H. J. Wollersheim, Eur. Phys. J. A **10**, 135 (2001).
[36] D. Belic, J. Besserer, C. Arlandini, J. de Boer, J. J. Carroll, J. Enders, T. Hartmann, F. Käppeler, H. Kaiser, U. Kneissl, M. Loewe, H. Maser, P. Mohr, P. von Neumann-Cosel, A. Nord, H. H. Pitz, A. Richter, M. Schumann, S. Volz, and A. Zilges, Nucl. Instrum. Methods Phys. Res. A **463**, 26 (2001).
[37] J. Blachot, Nucl. Data Sheets **86**, 151 (1999).
[38] D. Belic, C. Arlandini, J. Besserer, J. de Boer, J. J. Carroll, J. Enders, T. Hartmann, F. Käppeler, H. Kaiser, U. Kneissl, M. Loewe, H. J. Maier, H. Maser, P. Mohr, P. von Neumann-Cosel, A. Nord, H. H. Pitz, A. Richter, M. Schumann, S. Volz, and A. Zilges, Phys. Rev. Lett. **83**, 5242 (1999).
[39] S. Lindenstruth, A. Degener, R. D. Heil, A. Jung, U. Kneissl, J. Margraf, H. H. Pitz, H. Schacht, U. Seemann, R. Stock, and C. Wesselborg, Nucl. Instrum. Methods Phys. Res. A **300**, 293 (1991).
[40] P. von Neumann-Cosel, N. Huxel, A. Richter, C. Spieler, J. J. Carroll, and C. B. Collins, Nucl. Instrum. Methods Phys. Res. A **338**, 425 (1994).
[41] C. B. Collins, J. J. Carroll, K. N. Taylor, D. G. Richmond, T. W. Sinor, M. Huber, P. von Neumann-Cosel, A. Richter, and W. Ziegler, Phys. Rev. C **46**, 952 (1992).
[42] E. C. Booth and J. Brownson, Nucl. Phys. **A98**, 529 (1967).
[43] P. von Neumann-Cosel, A. Richter, C. Spieler, W. Ziegler, J. J. Carroll, T. W. Sinor, D. G. Richmond, K. N. Taylor, and C. B. Collins, Phys. Lett. B **266**, 9 (1991).

[44] U. Kneissl, H. H. Pitz, and A. Zilges, Prog. Part. Nucl. Phys. **37**, 349 (1996).
[45] U. E. P. Berg and U. Kneissl, Annu. Rev. Nucl. Part. Sci. **37**, 33 (1987).
[46] O. Bogdankevich and F. Nikolaev, *Methods in Bremsstrahlung Research* (Academic, New York, 1966).
[47] E. Bramanis, T. Deague, R. Hicks, R. Hughes, E. Muirhead, R. Sambell, and R. Stewart, Nucl. Instrum. Methods **100**, 59 (1972).
[48] H. J. Maier, R. Grossmann, H. U. Friebel, and D. Frischke, Nucl. Instrum. Methods Phys. Res. A **438**, 163 (1999).
[49] H. Maser, S. Lindenstruth, I. Bauske, O. Beck, P. von Brentano, T. Eckert, H. Friedrichs, R. D. Heil, R.-D. Herzberg, A. Jung, U. Kneissl, J. Margraf, N. Pietralla, H. H. Pitz, C. Wesselborg, and A. Zilges, Phys. Rev. C **53**, 2749 (1996).
[50] *Table of Isotopes*, 8th ed., edited by R. B. Firestone and V. S. Shirley (Wiley, New York, 1996).
[51] A. Wolpert, O. Beck, D. Belic, J. Besserer, P. von Brentano, T. Eckert, C. Fransen, R.-D. Herzberg, U. Kneissl, J. Margraf, H. Maser, A. Nord, N. Pietralla, and H. H. Pitz, Phys. Rev. C **58**, 765 (1998).
[52] H. Bartsch, K. Huber, U. Kneissl, and H. Sattler, Nucl. Instrum. Methods **121**, 185 (1974).
[53] D. Belic, Doctoral thesis, Universität Stuttgart, 2001.
[54] S. A. Karamian, C. B. Collins, J. J. Carroll, and J. Adam, Phys. Rev. C **57**, 1812 (1998).
[55] L. Lakosi and T. C. Nguyen, Nucl. Phys. **A697**, 44 (2002).
[56] M. Loewe, Doctoral thesis, Ludwig-Maximilians Universität München, 2002.
[57] V. G. Soloviev, Nucl. Phys. **A633**, 247 (1998).
[58] V. G. Soloviev, A. V. Sushkov, and N. Yu. Shirikova, Phys. At. Nucl. **64**, 1199 (2001); (private communication).
[59] P. M. Walker, G. Sletten, N. L. Gjørup, M. A. Bentley, J. Borggreen, B. Fabricius, A. Holm, D. Howe, J. Pedersen, J. W. Roberts, and J. F. Sharpey-Schafer, Phys. Rev. Lett. **65**, 416 (1990).
[60] P. M. Walker, D. M. Cullen, C. S. Purry, D. E. Appelbe, A. P. Byrne, G. D. Dracoulis, T. Kibedi, F. G. Kondev, I. Y. Lee, A. O. Macchiavelli, A. T. Reed, P. H. Regan, and F. Xu, Phys. Lett. B **408**, 42 (1997).
[61] P. Alexa, I. Hřivnáčová, and J. Kvasil, Acta Phys. Pol. B **30**, 1323 (1999).
[62] S. E. Woosley, D. H. Hartmann, R. D. Hofmann, and W. C. Haxton, Astrophys. J. **356**, 272 (1990).
[63] N. Prantzos, M. Hashimoto, M. Rayet, and M. Arnould, Astron. Astrophys. **238**, 455 (1990).
[64] R. Gallino, C. Arlandini, M. Busso, M. Lugaro, C. Travaglio, O. Straniero, A. Chieffi, and M. Limongi, Astrophys. J. **497**, 388 (1998).
[65] H.-T. Janka and W. Hillebrandt, Astron. Astrophys. **224**, 49 (1989); Astron. Astrophys., Suppl. Ser. **78**, 375 (1989).
[66] S. E. Woosley (private communication).
[67] A. Hektor, E. Kolbe, K. Langanke, and J. Toivanen, Phys. Rev. C **61**, 055803 (2000).
[68] E. Kolbe, K. Langanke, and P. Vogel, Phys. Rev. C **50**, 2576 (1994).
[69] E. Kolbe, K. Langanke, and P. Vogel, Nucl. Phys. **A652**, 91 (1999).
[70] J. D. Walecka, in *Semi-Leptonic Weak Interactions in Nuclei in Muon Physics*, edited by V. W. Hughes and C. S. Wu (Academic, New York, 1975).
[71] J. J. Cowan, F.-K. Thielemann, and J. W. Truran, Phys. Rep. **208**, 208 (1991); T. Rauscher and F.-K. Thielemann, At. Data Nucl. Data Tables **74**, 1 (2000).
[72] J. Toivanen, E. Kolbe, K. Langanke, G. Martinez-Pinedo, and P. Vogel, Nucl. Phys. A (to be published).
[73] M. Rayet, M. Arnould, M. Hashimoto, N. Prantzos, and K. Nomoto, Astron. Astrophys. **298**, 517 (1995).
[74] N. Klay, F. Käppeler, H. Beer, and G. Schatz, Phys. Rev. C **44**, 2839 (1991).
[75] K. T. Lesko, E. B. Norman, R.-M. Larimer, B. Sur, and C. B. Beausang, Phys. Rev. C **44**, 2850 (1991).